Original Article

Intranasal delivery of macrophage cell membrane cloaked biomimetic drug-nanoparticle system attenuates acute lung injury

Journal of Tissue Engineering
Volume 15: 1–19

DOI: 10.1177/20417314241287487
journals.sagepub.com/home/tej
Sage

Yue Zhao[1,2], Xin Shen[1,2], Yinqiang Fan[1], Ning Wei[1], Zijie Ling[2], Yinlian Yao[2], Shilong Fan[2], Jiahao Liu[1], Yiming Shao[1], Zhikun Zhou[1,2] and Hua Jin[1,2]

Abstract

Acute lung injury (ALI)/acute respiratory distress syndrome (ARDS), a life-threatening disease, is typically induced by uncontrolled inflammatory responses and excessive production of reactive oxygen species (ROS). Astaxanthin (Ast) is known for its powerful natural antioxidant properties, showcasing excellent antioxidant, anti-inflammatory, and immunomodulatory effects. However, its poor water solubility and bioavailability significantly limit its efficacy. Taking inspiration from biomimetic biology, this study developed a nasal drug delivery system comprising macrophage membrane (Mφ)-encapsulated Ast-loaded nanoparticles (Mφ@Ast-NPs) for the treatment of ALI. Mφ@Ast-NPs retain the original homing properties of Mφ, enabling targeted delivery to inflamed lungs and enhancing the anti-inflammatory effects of Astaxanthin (Ast). In vitro and in vivo, Mφ@Ast-NPs demonstrated excellent biocompatibility and safety, as evidenced by no hemolysis of red blood cells and no significant toxic effects on cells and major organs. To determine the inflammation-targeting of Mφ@Ast-NPs, both healthy and ALI mice were intranasally administered with Mφ@Ast-NPs, the results demonstrated that highly targeting to inflamed lungs and endothelia, while with minimal accumulation in healthy lungs and endothelia. Mφ@Ast-NPs effectively inhibited ROS production, enhanced Nrf2 expression and nucleus translocation, and reduced the levels of pro-inflammatory factors such as IL-1β, IL-6, and tumor necrosis factor-α (TNF-α) in LPS-induced RAW264.7 cells and ALI mice. Our study provided a safe and effective nasal delivery platform for pulmonary diseases, and this biomimetic nano-formulation of Ast could be as functional foods in the future.

Keywords

Acute lung injury, astaxanthin, macrophage membrane cloaked nanoparticles, reactive oxygen species, cytokine storm

Date received: 28 June 2024; accepted: 12 September 2024

[1]The First Dongguan Affiliated Hospital, Research Center of Nano Technology and Application Engineering, Dongguan Innovation Institute, Guangdong Medical University, Dongguan, China
[2]School of Pharmacology, Guangdong Medical University, Dongguan, China
[3]Laboratory Animal Center, School of Medical Technology, Guangdong Medical University, Dongguan, China

Corresponding authors:
Yinqiang Fan, The First Dongguan Affiliated Hospital, Research Center of Nano Technology and Application Engineering, Dongguan Innovation Institute, Guangdong Medical University, Dongguan 523808, China.
Email: gz8hfyq@126.com

Yiming Shao, The First Dongguan Affiliated Hospital, Research Center of Nano Technology and Application Engineering, Dongguan Innovation Institute, Guangdong Medical University, Dongguan 523808, China.
Email: sym@gdmu.edu.cn

Zhikun Zhou, The First Dongguan Affiliated Hospital, Research Center of Nano Technology and Application Engineering, Dongguan Innovation Institute, Guangdong Medical University, Dongguan 523808, China.
Email: zhouzhkun@126.com

Hua Jin, The First Dongguan Affiliated Hospital, Research Center of Nano Technology and Application Engineering, Dongguan Innovation Institute, Guangdong Medical University, Dongguan 523808, China.
Email: jinhua0413@gdmu.edu.cn

Introduction

ALI/ARDS typically arises from various conditions including pneumonia, sepsis, systemic infections, major surgeries, and multiple traumas. It is a common critical illness, characterized by prolonged hospitalization and high mortality rates. ALI/ARDS is considered a primary cause of death among intensive care unit patients, with mortality rates ranging from 30% to 70%.[1] Currently, there is no specific therapy for ALI/ARDS. In clinical practice, patients with ALI mainly receive supportive treatment with mechanical ventilation using a respirator. However, like any other invasive medical technology, mechanical ventilation can also lead to ventilator-associated lung injury, exacerbating ALI and its complications, with no markable decrease in mortality rates over the past few decades.[2] Antibiotics continue to stand as the mainstay treatment for ALI resulting from pneumonia; nonetheless, the emergence of drug-resistant and multidrug-resistant pathogens presents considerable hurdles in clinical care.[3] Glucocorticoids and antibody-based medications, though effective in dampening the cytokine storm and reducing lung tissue damage, frequently trigger varying degrees of systemic immunosuppression due to their non-specific anti-inflammatory actions.[4] Hence, delving into the pathogenesis, pinpointing targets, and devising efficacious strategies are crucial aspects to tackle in the management of ALI/ARDS.

Inflammatory cytokine storms and oxidative stress are pivotal in the pathogenesis of ARDS.[5] Inflammation-oxidation damage in the lungs heightens the permeability of the endothelial/epithelial barrier, enabling neutrophil infiltration and the release of cytotoxic factors, including various pro-inflammatory cytokines such as TNF-α, IL-6, IL-1β, and reactive oxygen species. This cascade further exacerbates the inflammatory response, magnifying tissue damage and pulmonary edema.[6] Therefore, inhibiting cytokine storm and oxidative stress is an efficacy strategy for the prevention and treatment of ALI/ARDS.

Astaxanthin (Ast) is a type of carotenoid, a natural pigment derived from crustaceans like shrimp, crab, and lobster. It's primarily found in their shells, shell membranes, and shell inner membranes. Natural Ast is known as one of the world's most potent natural antioxidants, which effectively scavenges oxygen free radicals within cells, boosting cell regeneration, maintaining organismal balance, and reducing the accumulation of aging cells.[7] Previous studies showed Ast has potential effects in the treatment of lung injury. Ast pretreatment could lead to a relief of lipopolysaccharide (LPS)-induced ALI, perhaps via suppressing ferroptosis[8] and reducing unstable iron accumulation in lung epithelial cells[9] and inhibit the inflammatory response, oxidative/nitrative stress, pulmonary apoptosis, and down-regulate NF-κB P65 expression[10] As a fat-soluble carotenoid, Ast exhibits poor water solubility and is susceptible to damage from external factors such as temperature, light, and oxygen. These limitations greatly hinder its application.[11] In the past decade, delivery systems utilizing complex coacervates, self-assembly, low-energy emulsification, and microfluidic methods have been developed to enhance the stability and biocompatibility of bioactive compounds like astaxanthin sourced from food.[12]

Nanoparticle drug delivery systems offer a range of advantages, including enhanced drug targeting, sustained and controlled release, improved drug uptake, prolonged half-life of drugs, reduced drug toxicity and side effects, and enhanced efficacy.[1] Despite their potential to improve drug properties such as controlled release and enhanced solubility, nanoparticles are often recognized as foreign entities by the body, leading to activation of clearance mechanisms by the reticuloendothelial system and compromising drug efficacy. To address these challenges, researchers have primarily focused on developing biomimetic nano-systems that are more compatible with drug delivery in the body. One of the most prominent techniques is the use of cell membrane-based biomimetic nanocarriers.[13] Cells, as the basic units of biological structure and function, provide a blueprint for designing biomimetic nanomaterials. Cell membrane cloaked biomimetic delivery systems not only retain the favorable properties of nanoparticles but also incorporate the natural receptors found on cell membranes. This innovative approach helps evade immune recognition and clearance, thereby extending the circulation time of the drug in the body. Additionally, it enables active targeting of nanodrugs, guided by the specific cell membranes they are designed to interact with.[14] Researchers have utilized cell membranes from red blood cells, platelets, tumor cells, neutrophils, and even bacterial cells to develop biomimetic nanoparticles with drug-loaded PLGA nanoparticles as cores.[15] These biomimetic nanoparticles have been successfully applied in the treatment and experimental research of various diseases such as tumors and inflammation. Macrophages, serving as the frontline of defense in the natural immune system, possess remarkable abilities to navigate physiological barriers, evade immune detection, and traverse intracellular pathways. Furthermore, they demonstrate the capacity to release potent pro-inflammatory cytokines, including tumor necrosis factor (TNF) and interleukin 6 (IL-6). Consequently, macrophage membrane-coated nanoparticles have emerged as a promising avenue in therapeutic development. In a comprehensive overview by Chu et al.,[16] the utility of macrophage membranes as a coating material for drug delivery was delineated, facilitating targeted tissue delivery for treating various ailments such as cancers, microbial infections, atherosclerosis, and inflammatory conditions. Shen et al.[17] discovered that nanoparticles enveloped in macrophage membranes, with specific binding of lipopolysaccharide (LPS) receptors on macrophage membranes, could capture and neutralize endotoxins, reduce the release of inflammatory factors, and effectively release drugs. This led to a significant

attenuation of the immune response in endotoxemia mouse models, thereby improving their survival rates. Thamphiwatana et al.[18] also observed that macrophage-encapsulated nanoparticles exhibit a similar antigenic profile to macrophages, possess the ability to bind endotoxins, reduce levels of pro-inflammatory cytokines, inhibit bacterial spread, and thereby extend the survival time of septic mice. Compared to traditional non-biomimetic nano-formulations, macrophage membrane-coated nanoparticles have demonstrated lower immunogenicity, higher targeting specificity, and better biocompatibility.[19]

In this study, we have successfully developed natural antioxidant-loaded PLGA NPs for managing ALI. These Ast-NPs were further functionalized with macrophage membrane (Mφ@Ast-NPs) to enable targeted delivery to inflammatory lesions in the lungs of ALI mice. The biocompatibility, targeting specificity toward inflammation, antioxidant capacity, and anti-inflammatory efficacy were evaluated both in vitro and in vivo. The biomimetic platform we synthesized (Mφ@Ast-NPs) exhibited highly efficient targeting and Ast delivery to alveolar macrophages, as evidenced by fluorescent imaging and flow cytometry analyses. The lung inflammation-targeting and accumulation of Mφ@Ast-NPs were further confirmed through IVIS imaging in septic mice. In an LPS-induced ALI mouse model, Mφ@Ast-NPs demonstrated significant therapeutic efficacy, as indicated by enhanced survival rates, reduced pulmonary permeability and cytokine release, and protection against organ damage. Moreover, Mφ@Ast-NPs displayed impressive antioxidant capabilities in both LPS-induced RAW264.7 cells and ALI mice. Astaxanthin may alleviate oxidative stress and reduce LPS-induced ALI by upregulating the Nrf2/HO-1 signaling pathway. This biomimetic nanoplatform could serve as a promising strategy for delivering natural antioxidant molecules, which could be functional foods in the future.

Materials and methods

Preparation of Ast loaded PLGA nanoparticles (Ast-NPs)

The Ast-NPs were synthesized using emulsification-and-evaporation method as our previous work described[20] with a little modification. Briefly, 20 mg Astaxanthin (Ast, purity: 98%, Shanghai Yuanye Bio-Technology Co., Ltd.) and 60 mg PLGA-PEG (lactide:glycolide 50:50, Sigma, USA) were co-dissolved in 5 mL of dichloromethane (Tianjin Damao Chemical Reagent Factory, China) as oil phase (O), 20 mL of PVA water solution (1%, w/w, Sigma) was as external water phase (W). Firstly, the O phase was ultrasonic for 40 s on ice bath to form the first emulsification. Then, the first emulsification was dropped in W phase and ultrasonicated for another 40 s to form the second emulsification. After that, the second emulsification was added to 100 mL water and stirred for 6 h for organic regent evaporation and nanoparticle hardening. Finally, the nanoparticles were harvested by centrifuging at 12,000 rpm for 20 min and washed three times using ultrapure water. The harvested NPs were stored at 4°C or lyophilized for long term storage.

Extraction of macrophage cell membrane (Mφ) and preparation of Mφ cloaked Ast-NPs (Mφ@Ast-NPs)

The extraction of cell membranes followed our previous protocol,[21] briefly, 5×10^7 RAW264.7 cells were collected using a cell scraper and centrifuged at 800 *g* for 5 min. The cells were then dispersed in 3 mL of hypotonic lysing buffer containing 50 mM Tris, 150 mM NaCl, 1% NP-40, 0.25% sodium deoxycholate, and 10% (v/v%) benzylsulfonyl fluoride. Then, the cells were kept in an ice bath for 15−30 min, followed by three-round of freeze−thaw processes (frozen in the −80°C and thawed at 37°C). The cell suspension was then centrifuged at 800 *g* for 15 min. The supernatant was collected and further centrifugated at 18,000 *g*, 4°C for 60 min. The final precipitate was collected as cell membranes, and the protein content was analyzed by bicinchoninic acid protein assay. Finally, the mixture of membrane vesicles and Ast-NPs were mixed and extruded via a Hand Extruder to obtain Mφ@Ast-NPs (Figure 1(a)).

Characterization of NPs

The size distribution and zeta potential of the nanoparticles were assayed using a Nano Particle Analyzer SZ-100 (Horiba Scientific, USA). Morphology of NPs were visualized by scanning electron microscopy (Philips Co, Holland).

A UV-vis spectrum (UV 6000) was used to scan free Ast, Ast-NPs, and Mφ@Ast-NPs, the UV absorption peak shift is not significant, which supposed that Ast was successfully encapsulated into NPs. To measure Ast loading rate, 10 mg lyophilized nanoparticles were dissolved in 1 mL of methanol, and then the amount of Ast in solution was determined by High Pressure Liquid Chromatography (HPLC). HPLC detection was performed using a C18 column (5 μm, 250 mm × 4.6 mm). Whereas the mobile phase, consisting of methanol and 0.1% acetic acid (88:12) (v/v), was maintained at a flow rate of 1.0 mL/min. The ultraviolet detector wavelength was 285 nm and the injection volume was 20 μL. The loading of Ast was calculated the concentration of Ast based on the standard curve of Ast at 285 nm. Fourier transform infrared (FTIR) spectroscopy (Nicolet 6700, Thermo, Waltham, USA) was used for analysis of the composition of the as-synthesized Mφ@Ast-NPs. To detect the efficiency of cell membrane coating, Bradford assay (Bio-Rad, CA, USA) was employed to measure the protein concentrations on the NPs.

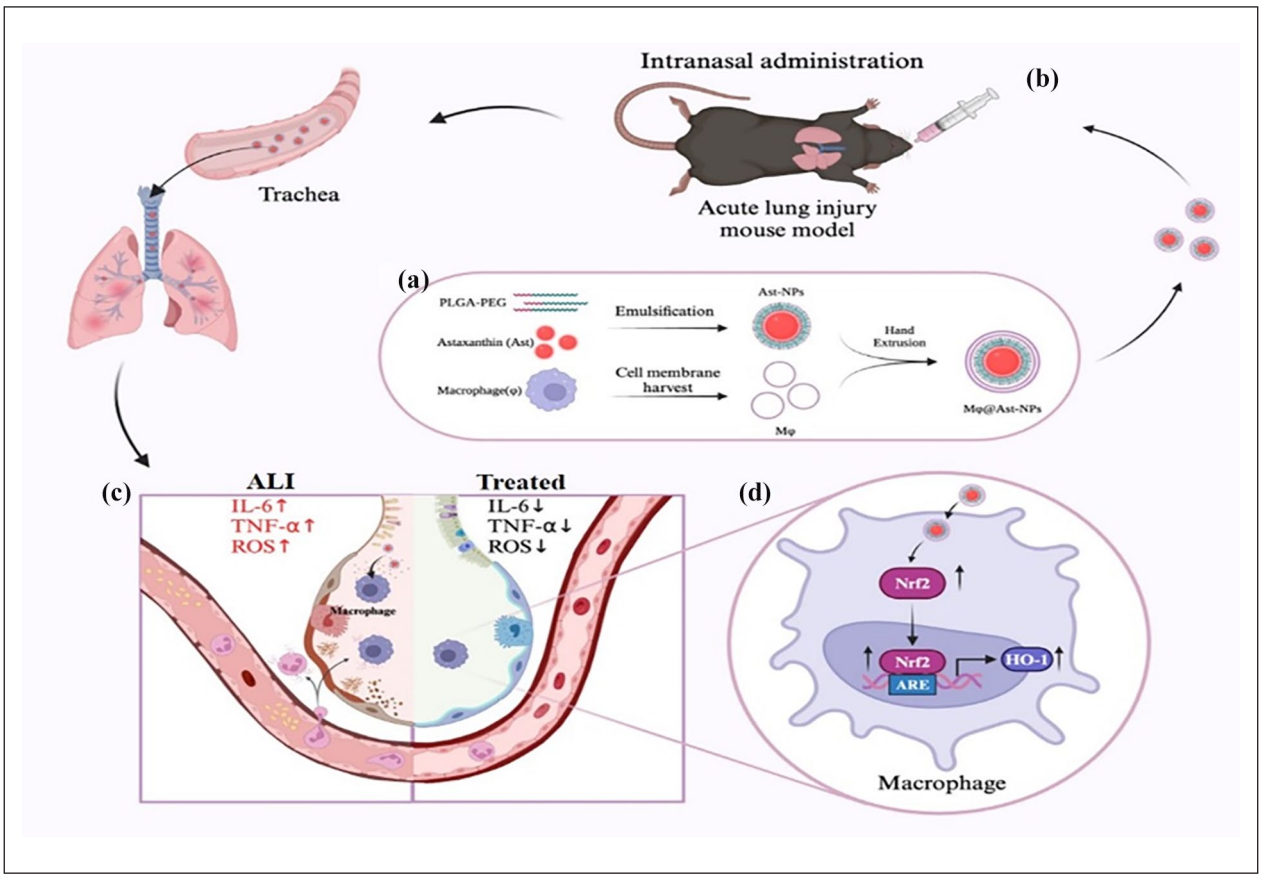

Figure 1. Schematic illustration of Mφ@Ast-NPs preparation and their treatment in ALI mice. (a) The Preparation of Ast-loaded PLGA nanoparticles cloaked with macrophage membrane (Mφ@Ast-NPs): At first, Ast-loaded PLGA NPs were prepared using emulsification-evaporation method. Then, macrophage cell membrane vesicles (Mφ) were extracted from the RAW264.7 cells. The harvested Ast-NPs were mixed with CM and extruded through a polycarbonate porous membrane to form Mφ@Ast-NPs. (b-c) The proposed illustration of nasally instillation (*i.n.*) administrated Mφ@Ast-NPs for the targeting and improving ALI treatment through inhibition of ROS-production and cytokine-secrection in the inflammatory lungs, and Nrf2 activation induced by Ast might contribute its ROS scavaging.

SDS-PAGE analysis of retention proteins from cell membranes and NPs

The macrophage membrane protein was prepared following the instructions of the Membrane and Cytosol Protein Extraction Kit P0033 (Beyotime, China). Briefly, the cells were scraped off from dishes after washing with pre-cooled PBS buffer and then added the reagents from Extraction Kit. A BCA protein assay kit (Solarbio, China) was used to determine the protein concentration of cell membrane. Macrophage membrane protein samples and Mφ@Ast-NPs were mixed with loading buffer (Beyotime, China) and denatured at 95°C. About 30 μg of protein samples was separated by 10% SDS-PAGE gel, and then, the gel was stained with Coomassie Blue for 2 h and decolored overnight for imaging.

In vitro targeting and biodistribution of the NPs

Due to the weak autofluorescence of Ast, Cumarin 6 (C6) was co-loaded into the Ast-NPs as a fluorescent marker. RAW264.7 cells and human umbilical vein endothelial cells (HUVECs) were provided by the Cell Library of Guangdong Provincial Key Laboratory of Medical Molecular Diagnostics, Guangdong Medical University. The cells were cultured in DMEM (Gibco, USA) with 10% fetal bovine serum (Gibco, USA) containing 100 μg/mL streptomycin and 100 IU/mL penicillin at 5% CO_2 and 37°C. The cells were cultured with C6/Ast-NPs for 4 h, and then washed twice with PBS to remove unbound nanoparticles followed by trypsinization. Flow cytometry analysis was performed at FITC channel. Results were expressed in terms of mean fluorescence intensity (MFI) of C6 in cells.

For further intracellular location determination, the cells were cultured with NPs for 2 h, then, stained with DAPI (Thermo Scientific, Waltham, MA, USA) to locate the nucleus and sealed the cells with glycerol before imaged under a laser confocal microscope.

CCK8 assay cell viability

To examine the effects of different formulations of Ast on RAW264.7 cells, the CCK8 (Zeta life, CA, USA) assay

was carried out to assess the cell viability and proliferation. In brief, RAW264.7 cells were plated in a 96-well plate at a density of 1×10^4 cells/well. Cells were treated with different concentrations of Ast, Ast-NPs, or Mφ@Ast-NPs for 24 h. Then, CCK8 assay was performed according to the manufactures' instructions.

Lactate dehydrogenase (LDH) cytotoxicity assay

According to the LDH cytotoxicity assay kit (Beyotime, C0016) to assess LDH activity in supernatants of RAW264.7 cells, indicating the extent of cell membrane disruption. Absorbance at 490 nm was measured using a Bio-Rad plate reader.

In vitro ROS level assay

The RAW264.7 cells suspension was seeded into 6-well plates (10^5 cells/well) and cultivated for 24 h. Next, different formulations of Ast were added to the cells for 24 hours. The cells were harvested to incubate with DCFH-DA (Sigma-Aldrich, St. Louis, MO, USA) for 30 min in dark at 37°C and washed twice with PBS. The MFI of DCFH-DA in cells was measured by flow cytometer at FITC channel.

Immunocytochemistry analysis

RAW264.7 cells were seeded on coverslips overnight. After treated with drugs and incubated for indicated time, the cells were stimulated with LPS for 24 h, followed by 4% PFA fixation for 20 min. The cells were permeabilized and stained with the indicated primary antibodies (Nrf2, Cell Signaling Technology, Boston, MA, USA) at 4°C overnight. The cells were incubated with fluorescence-conjugated secondary antibodies (Alexa Fluor® 488, Abcam, Cambridge, UK) for 2 h, followed by incubation with phalloidin (Cytoskeleton Inc, Denver, CO, USA) and DAPI for 15 min. Finally, cytoskeleton and protein expression were visualized by a confocal fluorescence microscopy system (Leica TCS SP8, Leica Microsystems, Wetzlar, Germany).

Macrophage polarization changes induced by Ast

About 15 μg/mL of Ast or Mφ@Ast-NPs were added into RAW264.7 cells, after 2 h, IL4 (20 ng/mL) or LPS (200 ng/mL) were also added to induce M2-type or M1-type, at 24 h post Ast treatment, the cells were harvested and isolated RNA for RT-qPCR test.

Animal study

About 8- to 12-week-age female C57/6J mice were purchased from SPF biotechnology co., LTD, Beijing, China. Experimental procedures using mice in this work were reviewed and approved by the ethical review board of Guangdong Medical University (GDY2202402). All the experiments were performed in accordance with relevant guidelines and regulations of Animal Ethics Committee of Guangdong province, China.

In vivo targeting and biodistribution of Ast-NPs

LPS-induced septic mice were intransal (*i.n.*) administered with 50 μL of Ast-NPs or Mφ@Ast-NPs, with indocyanine green (ICG) loaded into the NPs as the fluorescent marker. For semiquantitative analysis, the image and fluorescence intensities of mice were collected at 2, 4, and 8 h after intronasal (*i.n.*) administration of NPs. The mice were divided into three groups: basal, ICG/Ast, and Mφ@ICG/Ast group, three mice for each group for each time point, total 27 mice in this assay. The mice were anesthetized and determined using anesthesia system (contains: isoflurane and oxygen) of the Kodak Multi Mode Imaging System.

Lung mononuclear cells isolation

To further analysis the NPs endothelia targeting, the ALI mice were *i.n.* administrated with coumarin six-loaded NPs, after 4 h, the mice were anesthetized using CO_2 and sacrificed, then, the lungs were collected and isolated all the cells to determine the uptake of NPs using flow cytometry. Healthy mice without LPS treatment were also *i.n.* with Mφ@Ast-NPs served as healthy control group. The mice were divided into three groups: basal, ICG/Ast, and Mφ@ICG/Ast group, three mice for each group, total 12 mice were required in this assay. Lung mononuclear cells were prepared as previously described.[22] Briefly, lung tissues were sliced into small pieces and incubated at 37 °C for 45 min with collagenase IV (1 mg/mL; Life Technologies) in RPMI-1640 medium (HyClone) supplemented with 5% fetal bovine serum (FBS; HyClone), and cells were isolated by gradient centrifugation over 38% Percoll (GE Healthcare Life Sciences). After erythrocyte lysis with ACK lysis buffer (Gibco), the cells were harvested for analyses.

Also, lung tissues were isolate and rinsed thoroughly with PBS and embedded in Optimal Cutting Temperature compound (Sukura, Japan). Sections (5–10 μm) were stained with DAPI to locate the nuclei. Images were acquired using a Leica SP8 confocal microscope.

LPS-induced ALI mouse model and experimental groups

The mice were randomly divided into five groups (five mice/group), total 25 mice were required in this assay. After *i.n.* administrated with Ast (400 μg/kg), Ast-NPs (400 μg/kg), Mφ@Ast-NPs (400 μg/kg, calculating based on the loading of Ast in the NPs), or Vehicles (PBS containing 5% DMSO), separately. Three hours later, mice were i.p. injected with LPS (Beijing Solarbio Science & Technology

Co., Ltd.) at 5.0 mg/kg in 50 μL PBS. After 24 h, mice were anesthetized using a Ketamine/xylazine cocktail (Contains: 87.5 mg/kg Ketamine and 12.5 mg/kg Xylazine) with intraperitoneal injection, and collected samples (blood, bronchoalveolar lavage fluid, lung tissues, etc.).

Assay of ROS level in lungs and livers

The mice were divided into five groups: healthy mice, LPS + PBS, LPS + Ast, LPS + Ast-NPs, and LPS + Mφ@ Ast-NPs, three mice for each group, total 15 mice were required in this assay. The mice were anesthetized and perfused systemic blood before collected tissues. The lungs and livers were removed from the mice and immediately washed with PBS, and then submersed in DMEM medium with 100 μM DCFH-DA for 30 min at 37 °C in the dark. After washing twice with DMEM medium, the tissues were sunk in Phenol red-free medium and imaged using a Small Animal Live Imaging System (Eastman Kodak Co. USA).

Survival rate

The mice were i.p. administrated with lethal dose of LPS (8 mg/kg) challenge, after 3 h, the mice were *i.n.* administrated with different formulations of Ast (400 μg/kg) at once/8 h. During the whole experimental process, the mice were given normal access for water and food, and monitored four times a day for 7 days. Moribund mice were identified and euthanatized using CO_2 followed with cervical dislocation. On day 7, all the survived mice were euthanatized. The mice were divided into five groups: healthy mice, LPS + PBS, LPS + Ast, LPS + Ast-NPs, and LPS + Mφ@Ast-NPs, 10 mice for each group, total 50 mice were required in this assay.

Pro-inflammation cytokines assay

Elisa assay. Inflammatory cytokines in plasma and bronchoalveolar lavage fluid (BALF), including IL-1β and TNF-α, were assessed by ELISA kits according to the protocols provided by the manufacture (Jiangsu Meimian Industrial Co., Ltd).

Western blot

Immunoblotting analysis of proteins in RAW 264.7 cells was performed in the lysis buffer containing sodium dodecyl sulfate lysis buffer (Beyotime, Shanghai, China) and protease and phosphatase inhibitor cocktail (Thermo Fisher, USA) for 30 min. The protein concentration was assessed with a BCA assay kit (Beyotime, Shanghai, China). Protein extracts were separated on sodium dodecyl sulfatepolyacrylamide gel electrophoresis (8%–12% gels) and blotted onto Nitrocellulose membranes (Pall Corporation, NY, USA). After blocking with 5% fat-free milk, the membranes were incubated overnight at 4°C with the following primary antibodies: Nrf2 (1:1000, 80593, Proteintech, IL, USA), HO-1 (1:1000, ab13248, Abcam, Cambridge, UK), p62 (1:1000, ab155686, Abcam), and β-Actin (1:1000, cs8432, Santa Cruz Biotechnology, TX, USA) and secondary antibodies: Anti-rabbit IgG, HRP-linked Antibody (1:2000, 7074S, Cell Signaling Technology, MA, USA) and Anti-mouse IgG, HRP-linked Antibody(1:2000, 7076S, Cell Signaling Technology). Blots were visualized by Western Lumax Light Superior (310208, Zeta life).

Real-Time fluorescent quantitative PCR (RT-qPCR)

The RNA from colon tissue samples was extracted using the Trizol isolation reagent according to the manufacturer's directions. Reverse transcription reaction was conducted using Transcriptor First Strand cDNA Synthesis Kit (Roche, Inc., Basel, Switzerland). Quantitative real-time PCR analysis was performed using real-time PCR ViiATM7 with SYBR Green master mix (Roche, Inc., Basel, Switzerland). The relative expressions of mRNA were calculated using the $2^{-\triangle\triangle Ct}$ comparative method. The primers were used as follows:

TNF-α, forward primer: GTCAGGTTGCCTCTGT CTCA,

reverse primer: TCAGGGAAGAGTCTGGAAAG;

IL-6, forward primer: TAGTCCTTCCTACCCCAAT TTCC,

reverse primer: TTGGTCCTTAGCCACTCCTTC;

GAPDH, forward primer: AGGTCGGTGTGAACGGA TTTG,

reverse primer: TGTAGACCATGTAGTTGAGGTCA;

IL-1β, forward primer: GAAATGCCACCTTTTGA CAGTG;

reverse primer: TGGATGCTCTCATCAGGACAG;

IL-12, forward primer: CCCTTGCCCTCCTAAA CCAC;

reverse primer: AAGGAACCCTTAGAGTGCTTACT;

iNOS: forward primer: TACTGAGACAGGGAAG TCTGAA,

reverse primer: AGTAGTTGCTCCTCTTCCAAGGT;

Arg1, forward primer: CTCCAAGCCAAAGTCC TTAGAG,

reverse primer: AGGAGCTGTCATTAGGGACATC;

IL-10, forward primer: GCTCTTACTGACTGGC ATGAG,

reverse primer: CGCAGCTCTAGGAGCATGTG.

Histology

Lung tissues were fixed by 5 min of instillation of 10% formalin through trachea catheterization at a pressure of 15 cm H_2O, and then fixed in 10% formalin at room temperature for 48 h. Then lungs were embedded in paraffin, cut into 5 μm sections, and stained with hematoxylin and eosin (H&E).

In vivo biosafety of different formulations of Ast

The main organs originated from different treated ALI mice were stained with hematoxylin and eosin (H&E) and the lung injury score was assessed by five easily identifiable pathological processes according to the previous report.[23] The levels of alanine transaminase (ALT) and aspartate transaminase (AST) of liver homogenate in each group were also determined using the assay kits (C010-2-1, Nanjing Jiancheng Bioengineering Institute, China).

Statistical analysis

Results are expressed as mean ± SEM Statistical significance was determined by one-way ANOVA with a Games-Howell post hoc analysis for multiple-group comparisons. Two-group comparisons were analyzed by the two-tailed unpaired Student's *t*-test. Figures 3(b) and (c) used Student's *t*-test, and all the other statistics used ANOVA.

Results and discussion

Synthesis of Mφ membrane cloaked biomimetic nanoparticles

The inflammatory microenvironment in (ALI/ARDS) is characterized by an uncontrolled cytokine storm and the overproduction of reactive oxygen species (ROS).[24] In this context, the natural antioxidant Astaxanthin (Ast) is administered to the inflamed organs to neutralize excessive ROS.[25] As depicted in Figure 1(a), the synthesis of macrophage membrane-coated PLGA nanoparticles for Ast encapsulation involves several steps: Initially, a conventional emulsification-evaporation technique is employed to fabricate the PLGA nanoparticles, with Ast incorporated into the oil phase to yield Ast-loaded PLGA nanoparticles. Subsequently, these nanoparticles are combined with RAW264.7 macrophage membrane vesicles and extruded through a polycarbonate porous membrane, resulting in the formation of macrophage-cloaked Astaxanthin nanoparticles (Mϕ@Ast-NPs). The subsequent i.n. administration of these nanoparticles effectively delivers Ast to the lungs affected by ALI, thereby minimizing systemic off-target effects, as illustrated in Figure 1(b).This strategy leverages the synergistic effects of the Mϕ membrane and Ast to effectively target macrophages, reducing the expression of reactive oxygen species (ROS) and pro-inflammatory cytokines such as interleukin-1 beta (IL-1β), interleukin-6 (IL-6), and tumor necrosis factor-alpha (TNF-α), while also activating Nrf2-associated proteins (Figure 1(c)).

Characterization of Mφ@Ast-NPs

The Nano Particle Analyzer SZ-100 (Horiba Scientific) and scanning electron microscope (SEM) were employed for the characterization of the size and morphology of Ast-NPs and Mϕ@Ast-NPs. As shown in Figure 2(a), the size of Ast-NPs was approximately 200 nm, which slightly increased to around 287 nm with the Mϕ membrane coating. Notably, the zeta potential of Ast-NPs was about −19 mV, indicating a tendency to aggregate easily. Conversely, after coating with the Mϕ membrane, the zeta potential of Mϕ@Ast-NPs decreased to approximately −31 mV, suggesting favorable dispersion of the nanoparticles (Figure 2(b)). The SEM image (Figure 2(c)) illustrated that both types of NPs exhibited a spherical and uniform morphology with a diameter of approximately 300 nm. These SEM findings further supported the effective dispersion of Mϕ@Ast-NPs, consistent with the Zeta potential results. In the FTIR spectroscopy analysis (Figure 2(d)), specific absorption peaks at 2948.1 cm^{-1} of PLGA and 974.9 cm^{-1} of Ast were observed in the Ast-loaded PLGA NPs, confirming the successful encapsulation of Ast into Mϕ@Ast-NPs. The UV-vis spectrum of the NPs was examined to assess the Ast loading. As depicted in Figure 2(h), the absorption spectrum of Ast exhibited characteristic peaks at 475 nm. The absorption peak of Ast-NPs and Mϕ@Ast-NPs was approximately 465 nm, closely resembling that of free Ast, indicating successful encapsulation of Ast into the NPs. The loading capacity of Ast in both Ast-NPs and Mϕ@Ast-NPs was 68%, calculated based on the standard curve of Ast at its UV absorption peak at 475 nm.

To confirm the coating of macrophage membrane vesicles (MφM) onto the Ast-NPs, the protein components of Mφ and Mφ@Ast-NPs were analyzed using SDS-gel electrophoresis[26]. As shown in Figure 2F, Mφ@Ast-NPs contained characteristic proteins preserved by Mφ membranes, providing strong evidence for the successful coating or conjugation of MφM proteins on the surface of the Ast-NPs. These findings support the biological functionality, such as inflammation-targeting, of the nanoparticles.

In vitro biocompatibility of different formulations of Ast

The rapidly evolving field of nanoparticle-based therapeutics has brought about significant advancements in the domain of nanomedicine.[27] These breakthroughs are meticulously crafted to overcome the inherent limitations of conventional treatments. A fundamental initial stride in the journey toward clinical implementation is

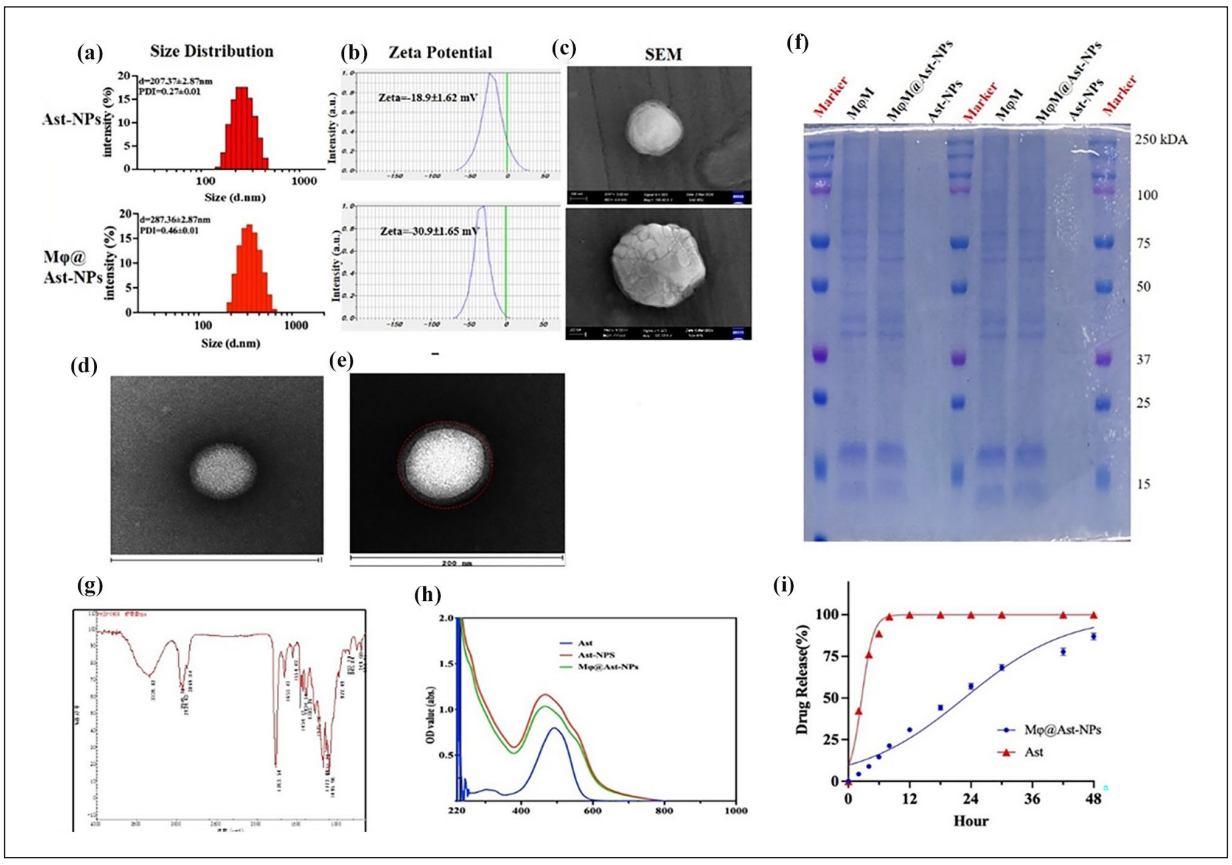

Figure 2. Characterizations of Mφ@Ast-NPs. (a) and (b) Size distribution, polydispersity index (PDI) and zeta potential of Ast-NPs and Mφ@Ast-NPs, respectively. (c) Representative morphology image of Ast-NPs and Mφ@Ast-NPs determined by scanning electron microscope (1 bar = 1 μm). (d and e) TEM image of (d) bare Ast-NPs and (e) Mφ@Ast-NPs. (f) SDS-PAGE protein analysis of macrophage cell membrane (MφM), Ast-NPs, and Mφ@Ast-NPs (the samples were determined at same protein concentrations). (g) FTIR analysis of Mφ@Ast-NPs. (h) UV-vis spectrum of free Ast, Ast-NPs, and Mφ@Ast-NPs indicated that Nar was encapsulated in Mφ@Ast-NPs, which shown by the similar absorption peaks at around 475 nm. (i) In vitro release kinetics of free Ast and Mφ@Ast-NPs at 37°C in PBS solution (pH = 6.5).

the validation of the biosafety and biocompatibility of emerging nanoparticle formulations. In this study, we utilized RAW264.7 cells to assess the potential cytotoxicity of various Ast formulations. The results of CCK8 and LDH assay (Figure 3(a) and (b)) depicts that free Ast exhibited a modest inhibitory impact on macrophage viability. Specifically, concentrations below 40 μg/mL did not induce cytotoxicity in macrophages, whereas a concentration of 100 μg/mL notably decreased cell viability by approximately 25%. Remarkably, even at high concentrations of 100 μg/mL or higher, both Ast-NPs and Mϕ@Ast-NPs showed no significant cytotoxic effects on RAW264.7 cells. These results imply that encapsulating Ast in nanoparticle formulations can effectively alleviate cytotoxicity, thereby bolstering the safety profile of Ast.

In ALI/ARDS, pulmonary macrophages serve as the guardians of the innate immune system, acting as the first line of defense against environmental threats.[28] These cells excel not only in recognizing pathogen-associated molecular patterns, thereby initiating innate immune responses and strengthening host defenses, but also play a significant role in the overall pathogenesis of ALI/ARDS. Their functions encompass the regulation of inflammatory processes and the promotion of tissue repair mechanisms within the pulmonary microenvironment.[29] Consequently, targeted drug delivery to alveolar macrophages is crucial for the resolution of ALI/ARDS. To enhance the visibility of Ast, which has weak fluorescence, coumarin 6 (C6) was co-loaded into the nanoparticles as a fluorescent marker. Following a 2-h co-culture, the nanoparticles successfully penetrated naïve RAW264.7 cells, as confirmed by fluorescent imaging (Figure 3(c and d)). Further investigations into the in vitro inflammation-targeting capabilities of Mϕ@Ast-NPs involved stimulating RAW264.7 cells with 1 μg/mL of LPS for 24 h to induce an inflammatory state. After a 2-h co-culture, a significantly greater amount of Mϕ@Ast-NPs entered the inflamed cells compared to Ast-NPs. Intriguingly, the uptake of Ast-NPs by LPS-stimulated cells exceeded that by naïve RAW264.7 cells, suggesting a

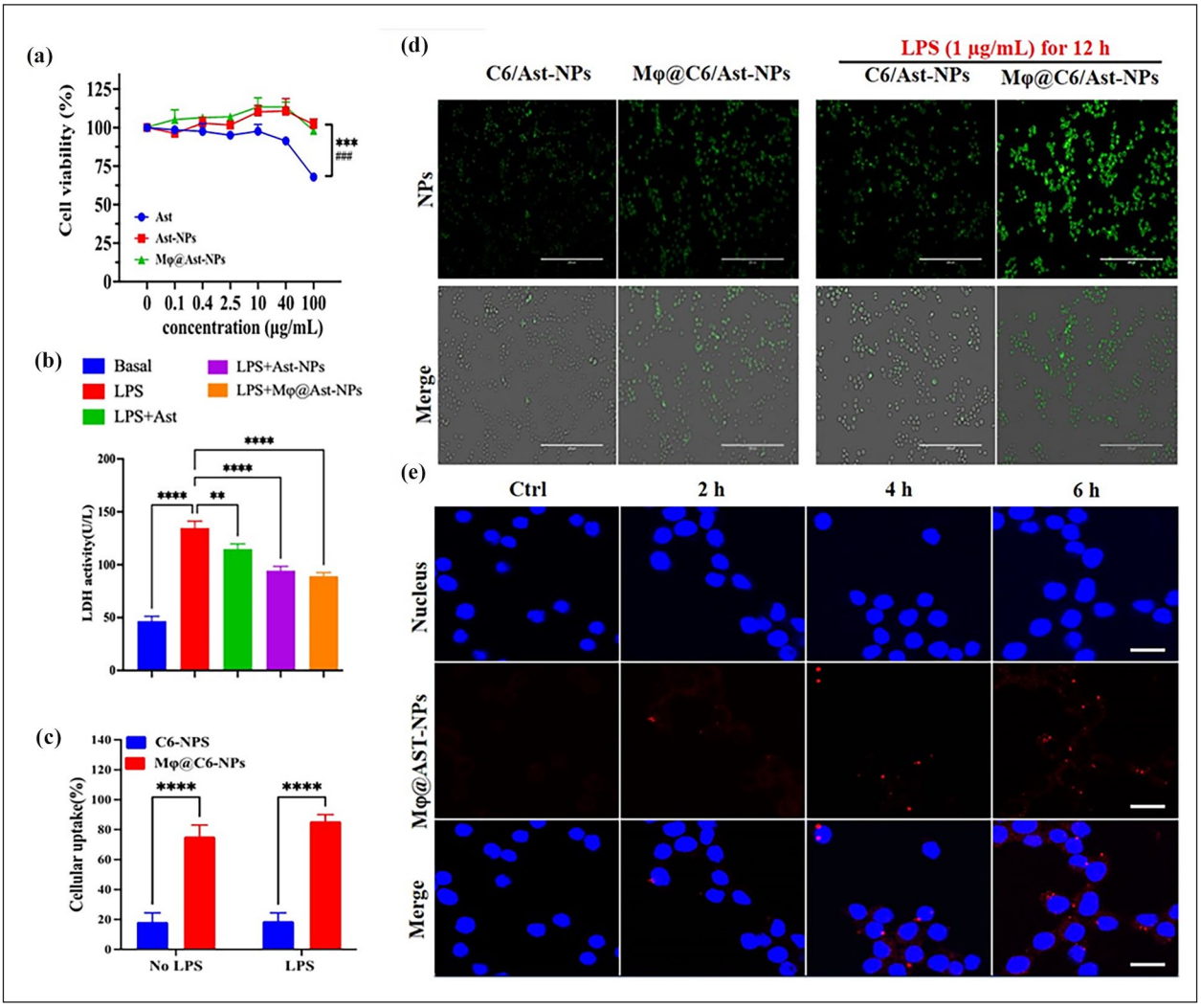

Figure 3. In vitro biocompatibility of different formulations of Ast. (a and b) Cell viability of RAW264.7 treated with different formulations of Ast at different concentrations for 24 h determined by CCK8 (a) and LDH assay (b). (c and d) Cellular uptake of NPs in RAW264.7 cells. Due to the weak fluorescence of Nar, Coumarin 6 (C6) was co-loaded into the NPs as fluorescent marker. (c) Quantitative analysis of mean fluorescence intensity (MFI) of intracellular C6 determined by flow cytometry. (d) The typical images of Cellular uptake of free C6/Ast-NPs or Mφ@C6/Ast-NPs in RAW264.7 cells co-cultured with NPs for 2 h. Scale bars: 200 μm. (e) Biodistribution of Mφ@C6/Ast-NPs (red color) in LPS-induced RAW264.7 cells: DAPI located the nuclear. Scale bars: 5 μm. ****$p < 0.0001$, ns, no significant differences ($n = 5$).

preference of Mϕ@Ast-NPs for targeting inflamed cells (Figure 3(c and d)). Confocal images further demonstrated the time-dependent entry of Mϕ@Ast-NPs into LPS-induced RAW264.7 cells (Figure 3e).

In vitro ROS scavenging activity of different formulations of Ast

Growing evidence has highlighted the pivotal role of reactive oxygen species (ROS) in the pathophysiology of ALI/ARDS. Both preclinical and clinical studies have suggested the potential benefits of antioxidants in mitigating ARDS. Therefore, the utilization of antioxidants for the treatment of ALI/ARDS holds considerable promise.[30] Flow cytometry analysis utilizing DCFH-DA (shown in Figure 4 (a, b, and d)) revealed that LPS significantly induced ROS generation in RAW264.7 cells, while free Ast, particularly Ast- NPs, effectively reduced ROS levels in the cells. Remarkably, Mφ@Ast-NPs exhibited the most pronounced ROS scavenging effect compared to the other treated groups. Furthermore, the results of live cell fluorescence imaging (Figure 4(c)) corroborated the findings from the flow cytometry analysis.

The nuclear factor E2-related factor 2 (Nrf2) is a widely recognized anti-oxidative transcription factor that plays a pivotal role in regulating oxidative stress responses. Acting as a master transcription factor, Nrf2 controls a diverse range of cytoprotective genes, including heme oxygenase-1

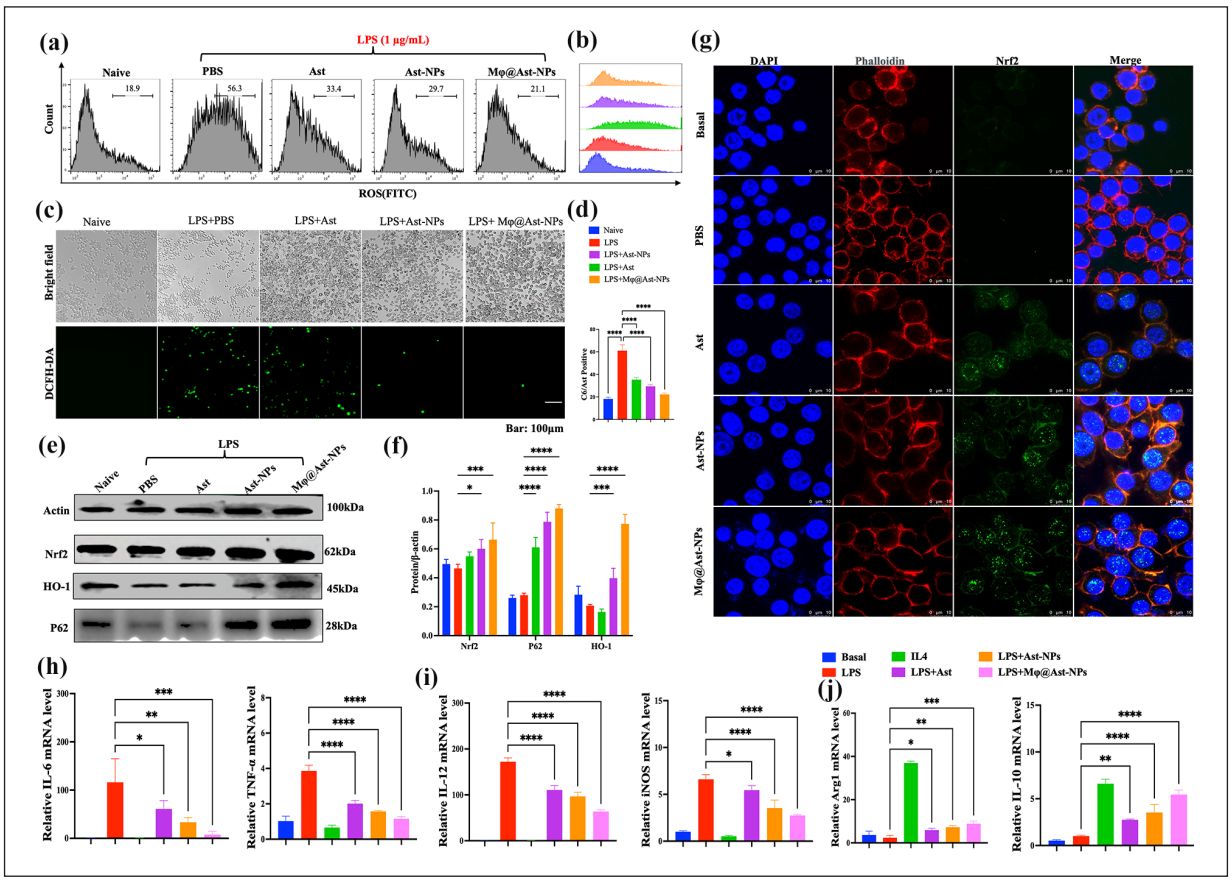

Figure 4. *In vitro* ROS scavenging activity of different formulations of Ast. (a-b, d) Flow cytometry (FCM) analysis of reactive oxygen species (ROS) level in RAW264.7 cells challenged with LPS (1 μg/mL) for 24 h. RAW264.7 cells pretreated with different formulations of Ast (400 μg/kg) 3 h before 1 μg/mL of LPS challenging. (c) The fluorescent pictures of RAW264.7 cells stained with DCFH-DA kits imaged by live cell imaging system. (e-f) Effects of Ast on the expression of Nrf2-related proteins: (e) Representative western blot analysis of Nrf2, P62, and HO-1 expression in total and nuclear proteins. (f) Quantitative analysis of the results in (e). (g) The effects of different formulations of Ast on Nrf2 nuclear localization. (h-j) To determine the effects of Ast on macrophage polarization, the cytokine levels (IL-6 and TNF-α), M1 marker (IL-12 and iNOS) and M2 marker (Arg1 and IL-10) were assayed using q-PCR. *$p < 0.05$, **$p < 0.01$, ***$p < 0.001$, ****$p < 0.0001$, ns, no significant differences ($n = 3$).

(HO-1). Numerous studies have highlighted the involvement of the Nrf2/HO-1 signaling pathway in pulmonary inflammatory conditions. The upregulation of Nrf2/HO-1 has been shown to reduce reactive oxygen species (ROS) production and inflammatory cytokines, thus significantly contributing to tissue protection.[31] Our previous investigations indicated that activating Nrf2/HO-1 with herbal ingredients like Oridonin could effectively alleviate ALI.[32] Multiple studies suggest that AST exhibits anti-aging properties by mitigating oxidative stress and inflammation through Nrf2 activation and NF-κB inhibition.[33] Consequently, AST shows promising potential for the treatment of lung diseases.[34] Li et al.[8] reported that AST attenuated ferroptosis via the Keap1-Nrf2/HO-1 signaling pathways in LPS-induced ALI. Our objective is to verify whether Ast-loaded biomimetic nanoparticles could enhance the activation of the Nrf2/HO-1 signaling pathway. Western blot analyses (Figure 4(e)) revealed that while macrophages exposed to LPS exhibited unaltered Nrf2 and HO-1 expressions, Ast upregulated both Nrf2 and HO-1, with Mφ@Ast-NPs showing the most significant enhancement among the four treated groups. Furthermore, as a critical scaffold and adaptor protein in the autophagy signaling pathway, p62 acts as a central hub facilitating the crosstalk between autophagy signaling and the Nrf2 pathway. The binding of Nrf2 to downstream antioxidant elements in the p62 promoter region can amplify p62 production, establishing a positive feedback loop. Additionally, p62 competitively binds to Keap1, promoting its clearance through the autophagy pathway and facilitating Nrf2 dissociation into the nucleus. Both western blot and confocal microscopy results (Figure 4(e) and (f)) indicated that while LPS-exposed macrophages showed unaltered P62 expression, Ast upregulated P62 levels and increased Nrf2 nuclear translocation. Moreover, Mφ@

Ast-NPs exhibited the most pronounced enhancing effect on both P62 and Nrf2 among the treated groups. These findings suggest that AST's inhibition of ROS production in macrophages may occur through the activation of the Nrf2/HO-1/p62 signaling pathway.

When exposed to various microenvironmental stimuli, macrophages exhibit high plasticity, primarily polarizing into the pro-inflammatory M1 phenotype and the anti-inflammatory M2 phenotype.[35] To determine the effects of different formulations of Ast on macrophage polarization, we assessed the markers of M1-type macrophages (pro-inflammatory), including IL-12 and iNOS, as well as the markers of M2-type macrophages (anti-inflammatory), such as Arg1 and IL-10. IL-4 or LPS were added to induce macrophages into M2 or M1 polarization, respectively, serving as control groups. As shown in Figure 4(h), LPS significantly induced the production of pro-inflammatory cytokines, IL-6 and TNF-α, whereas treatment with IL-4 or Ast resulted in a remarkable decrease in both IL-6 and TNF-α levels. Additionally, Ast or Mϕ@Ast-NPs effectively reduced the levels of M1-type markers (Figure 4(i)). Conversely, Ast or Mϕ@Ast-NPs significantly increased the levels of M2-type markers (Figure 4(j)). Notably, Mϕ@Ast-NPs exhibited more pronounced effects compared to free Ast. These results demonstrate that Ast or Mϕ@Ast-NPs inhibit the secretion of inflammatory factors, likely by promoting macrophage polarization toward the M2 phenotype.

In vivo biodistribution of different formulations of Ast in ALI mice

To confirm the specificity and retention of Mϕ@Ast-NPs in the context of pulmonary inflammation, indocyanine green (ICG) was integrated as a fluorescent label into the nanoparticles. The procedure and timeline for the in vivo targeting experiments are outlined in Figure 5(a). Initially, mice were intraperitoneally (i.p.) injected with LPS at a dose of 3.5 mg/kg to induce ALI. Subsequently, Ast/ICG-NPs or Mϕ@Ast/ICG-NPs were administered intranasally (*i.n.*) to monitor the distribution of the nanoparticles. As depicted in Figure 5(b), Mϕ@Ast/ICG-NPs mainly accumulated in the lungs of ALI mice, while Ast/ICG-NPs were primarily detected in the livers at 2, 4, and 8 h post-intranasal delivery. At 8 h post *i.n.* administration (Figure 5(c)), Mϕ@Ast/ICG-NPs exhibited a markedly higher fluorescence intensity in the lungs compared to the liver-targeted Ast/ICG-NPs. Analysis through the in vivo imaging system (IVIS) data (Figure 5(e) and (f)) indicated that the accumulation of Mϕ@Ast/ICG-NPs in the lungs was approximately five times greater than that of Ast/ICG-NPs. These results indicate that the incorporation of Mϕ membranes significantly boosts the targeting and retention of Ast-NPs in inflamed pulmonary tissues.

In vivo cellular uptake of NPs in lung tissue

The accumulation and internalization of nanomedicines in tissue lesions play a critical role in their therapeutic efficacy. Particularly, targeting and suppressing the activation of vascular endothelial cells are essential for reducing inflammation and vascular damage in the treatment of ALI. The experimental timeline is illustrated in Figure 6(a): In the LPS-induced mouse model, free C6-Ast or Mϕ@C6/Ast-NPs were intranasally administered for 4 h, following which the animals were anesthetized with CO2, and lung tissues were collected to evaluate intracellular nanoparticle (NP) uptake. Immunohistochemical analysis of frozen lung sections (Figure 6(b)) demonstrates a significantly higher presence of Mϕ@C6/Ast-NPs (shown by green fluorescence) within lung cells (identified by the blue fluorescence of DAPI staining the nuclei) and endothelial cells (identified by the red fluorescence of CD31 antibody staining for endothelia) compared to free C6/Ast. The results in Figure 6(b) highlight that the Mϕ membrane coating substantially improves NP delivery into lung cells. Specifically, the accumulation of Mϕ@NPs in lung cells was approximately three times greater than that of the unmodified C6/Ast-NPs (Figure 6(b) and (c)).

Furthermore, the flow cytometry analysis revealed that the Mϕ membrane coating significantly enhanced NP delivery in lung cells and endothelial cells (Figure 6(d)–(g)). The accumulation of Mϕ@NPs in lung cells was approximately three times higher than that of unmodified NPs (Figure 6(d) and (e)). Moreover, to assess the inflammation-targeting potential of NPs, the cellular uptake of Mϕ@Ast/C6-NPs in cells from both ALI lungs and healthy lungs was compared. Remarkably, minimal accumulation and retention of Mϕ@Ast/C6-NPs were observed in lung cells and endothelial cells (last panel in Figure 6(d) (f)) from healthy lungs. In contrast, a substantial accumulation of Mϕ@Ast/C6-NPs was observed in lungs from ALI mice, with the uptake of Mϕ@Ast/C6-NPs significantly surpassing that of unmodified Ast/C6-NPs, underscoring the enhanced inflammation-targeting capability conferred by the Mϕ membrane coating.

Collectively, the in vivo data (Figures 5 and 6) indicate that the intranasal delivery of Mϕ-coated nanoparticles can significantly enhance the specific targeting of nanoparticles to the inflamed lungs and cells. In the lungs of healthy mice, minimal accumulation and retention of Mϕ@Ast/C6-NPs are observed, suggesting the exceptional inflammation-targeting capability and favorable biosafety profile of these biomimetic nanoparticles.

Anti-inflammation effects of different formulations of Ast

To demonstrate the therapeutic efficacy and anti-inflammatory activity of biomimetic targeted delivery, mice

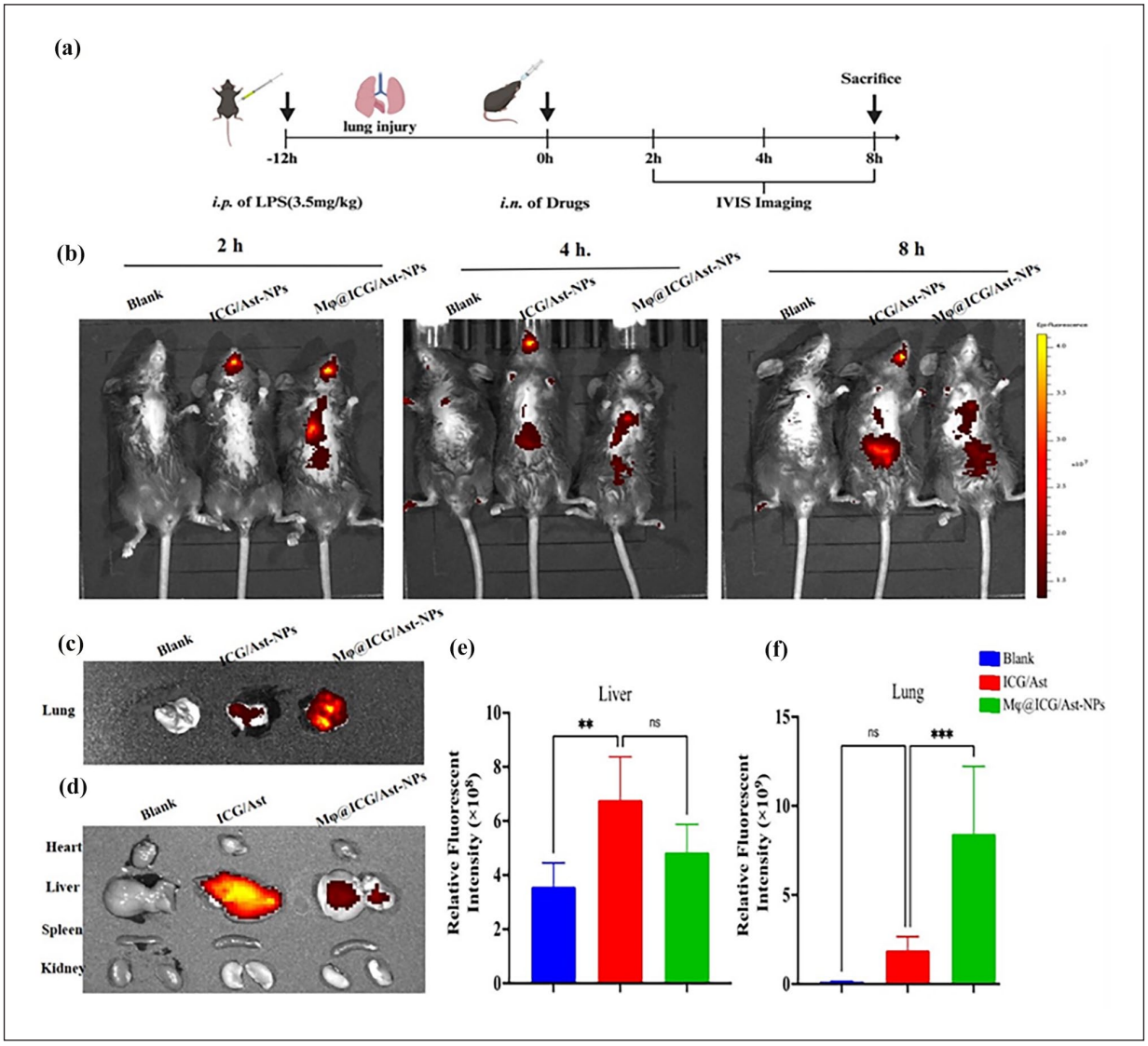

Figure 5. In vivo biodistribution of different formulations of Ast in ALI mice. Indocyanine green (ICG) was co-loaded into the NPs as a fluorescent marker in vivo. (a) Time-axis of in vivo imaging determination: the mice were intraperitoneally (i.p.) administrated with LPS (3.5 mg/kg body weight) to induce sepsis model, the mice were *i.n.* administrated with different modified of Ast-NPs at 12 h post LPS challenge. The mice were sacrificed and collected main organs at designated time post LPS challenge. (b) Representative IVIS imaging of balnk, ICG/Ast-NPs or Mφ@ICG/Ast-NPs distributed in ALI mice at 2, 4, and 8 h after intranasal administration of different compounds. (c) Relative accumulations of ICG/Ast-NPs in lung tissues measured with Living Image 4.5 software, which demonstrated that CM cloaked NPs significantly promoted the accumulation of ICG/Ast-NPs in lungs of ALI mice. (d) Typical fluorescence imaging of main organs originated from ALI mice after i.n. of CM@ICG/Ast-NPs for 8 h. *$p < 0.05$, **$p < 0.01$, ***$p < 0.001$, ****$p < 0.0001$, ns, no significant differences ($n = 3$).

were exposed to LPS at a dose of 3.5 mg/kg to induce ALI. Three hours later, the mice received intranasal administration of phosphate-buffered saline (PBS), free Ast (400 μg/kg body weight), or Ast-loaded nanoparticles, Mϕ@Ast-NPs (equivalent to 400 μg/kg of Ast), for three doses spaced 8 h apart, and were euthanized 24 h post the LPS challenge for analysis (the experimental timeline is illustrated in Figure 7(a)). It is widely acknowledged that preventing or alleviating the cytokine storm may constitute a vital strategy in saving the lives of patients with severe pneumonia. The total cell counts and protein levels in the BALF of the LPS-exposed group were significantly elevated compared to those in the healthy control group. Post Ast intervention, a significant reduction in both total cell counts and protein levels in the BALF was observed (as shown in Figure 7(b) and (c)). Levels of pro-inflammatory cytokines, including IL-6, TNF-α, and IL-1β, in plasma and lung tissue were evaluated using Elisa and RT-qPCR following the treatments (depicted in Figure 7(d)–(f)).

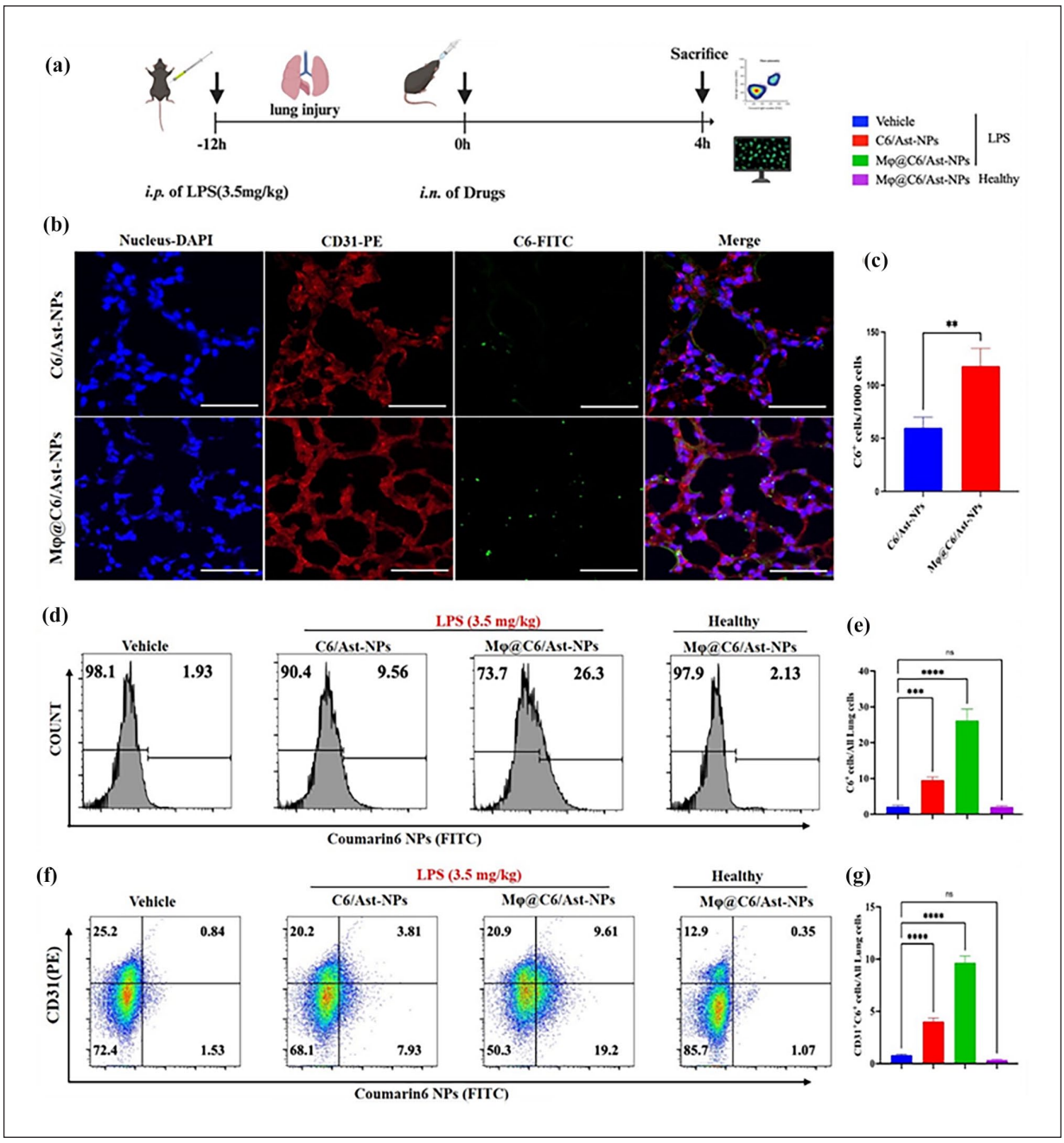

Figure 6. *In vivo* cellular uptake of NPs in lung cells assayed by Flow cytometry. Coumarin 6 (C6) was co-loaded into the NPs as a fluorescent marker *in vivo*. (a) Time-axis of *in vivo* targeting determination: the mice were *i.p.* administrated with LPS (3.5 mg/kg body weight) to induce sepsis model, after 12 h, the mice were *i.n.* administrated with different modified Ast-NPs. The mice were sacrificed and collected main organs at 4 h after NPs administration. (b-c) The fluorescent pictures and quantitative of C6/Ast-NPs or CM@C6/Ast-NPs (green color) in lung sections at 4 h *i.n.* administration (blue color of DAPI to locate nucleus, red color of CD31 antibodies to locate endothelial cells). (d-g) Flow cytometry assay the uptake of NPs in lung cells (b-c) and endothelia cells (d-e) in ALI or healthy lungs. Data are expressed as mean ± SD (n = 4). $^{**}p < 0.01$, $^{***}p < 0.001$, $^{****}p < 0.0001$, ns, no significant differences (n=5).

Although previous studies[36] have demonstrated that intravenous administration of free Ast at a dosage of >20 mg/kg daily for seven consecutive days can mitigate the cytokine storm in ALI, the therapeutic efficacy was limited in our experimental mouse model of ALI at a dose of 400 μg/kg. Both free Ast and Ast-loaded nanoparticles treatments showed only marginal reductions in cytokine levels at this lower dosage.

Encouragingly, these inflammatory factors were significantly decreased after *i.n.* of Mϕ@Ast-NPs, indicating that the cytokine storm was efficiently suppressed by the targeted delivery of Ast using the Mφ membrane cloaked

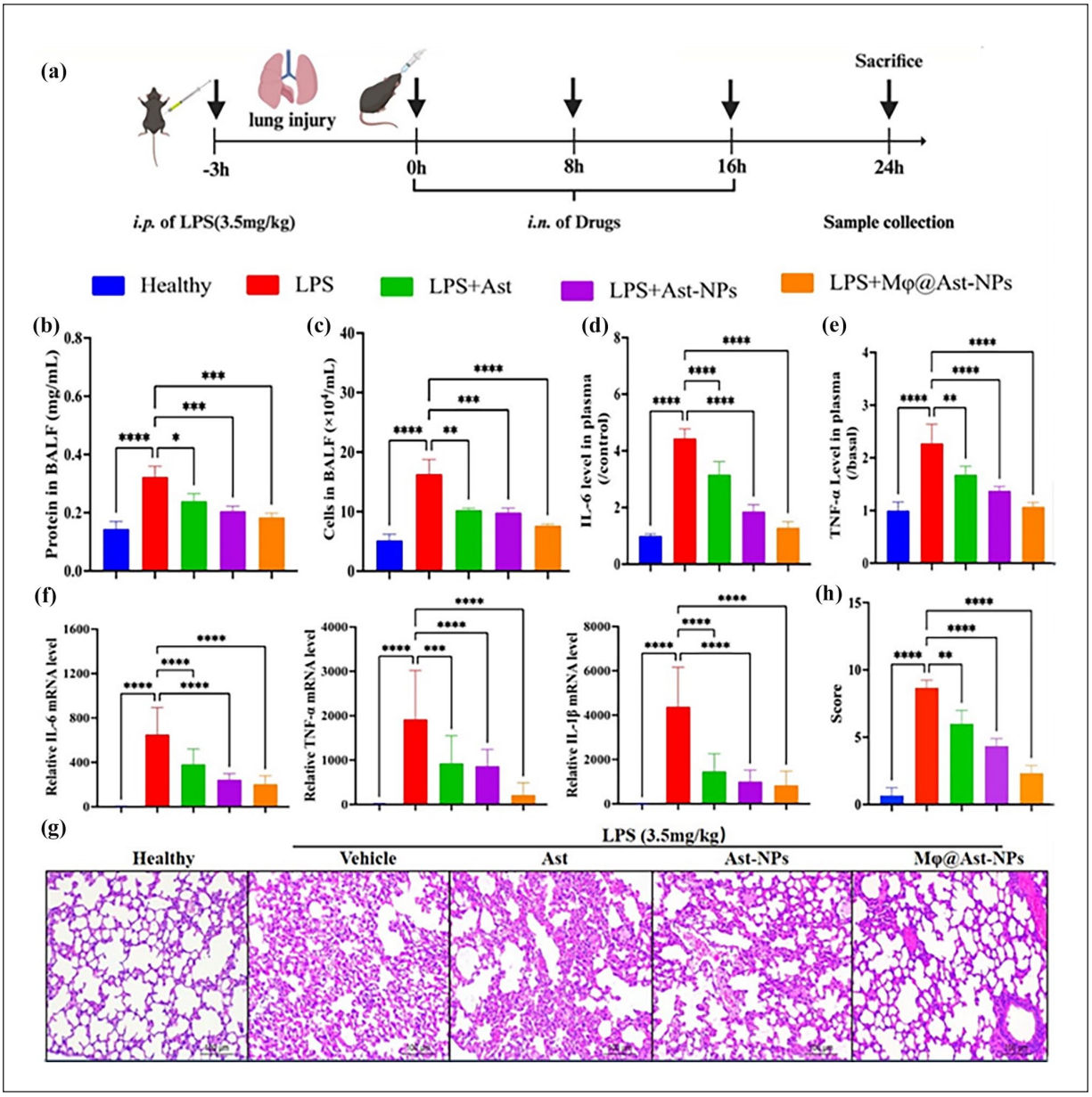

Figure 7. Anti-inflammation effects of different formulations of Ast. (a) Time axis of LPS-induced ALI and the timing of treatment: Mice were adaptively fed for one week, then *i.p.* of LPS to induce ALI model, after 3 hours, the mice were *i.n.* administrated with different formulations of Ast at 400 μg/kg for 3 times (8 h for single dose). At 24 h post LPS challenge, the mice were sacrificed and collected BALF, blood, and lung tissues. (b-c) Protein level and total cell counts in BALF. (d-e) Levels of pro-inflammation cytokines (IL-6, TNF-α) in mouse plasma determined by Elisa. (f) RNA levels of IL-6, TNF-α and IL-1β in ALI lungs determined by q-PCR. (g-h) Representative micrographs and the lung injury score of lung tissue cross-sections at 24 h post-LPS challenge stained by h&e. Scale bar: 100 μm. *$p < 0.05$, **$p < 0.01$, ***$p < 0.001$, ****$p < 0.0001$, ns, no significant differences (n=5).

biomimetic NPs. Moreover, histological sections stained with hematoxylin and eosin (H&E) further confirmed the presence of excessive pulmonary edema, alveolar inflammatory cell infiltration, and alveolar injury in the septic mice treated with PBS (Figure 7(g-h)). In the group treated with Mϕ@Ast-NPs, the inflammatory cell infiltration was significantly reduced compared to both the free Ast or non-modified Ast-NPs treated groups. Overall, these results demonstrate that Mϕ@Ast-NPs effectively inhibit inflammatory cell infiltration, alleviate pulmonary edema, and mitigate the cytokine storm in ALI mice.

In vivo ROS scavenging activity of different formulations of Ast

Furthermore, we observed that treatment with Mϕ@Ast-NPs significantly suppressed the generation of reactive oxygen species (ROS) in the lungs and livers during

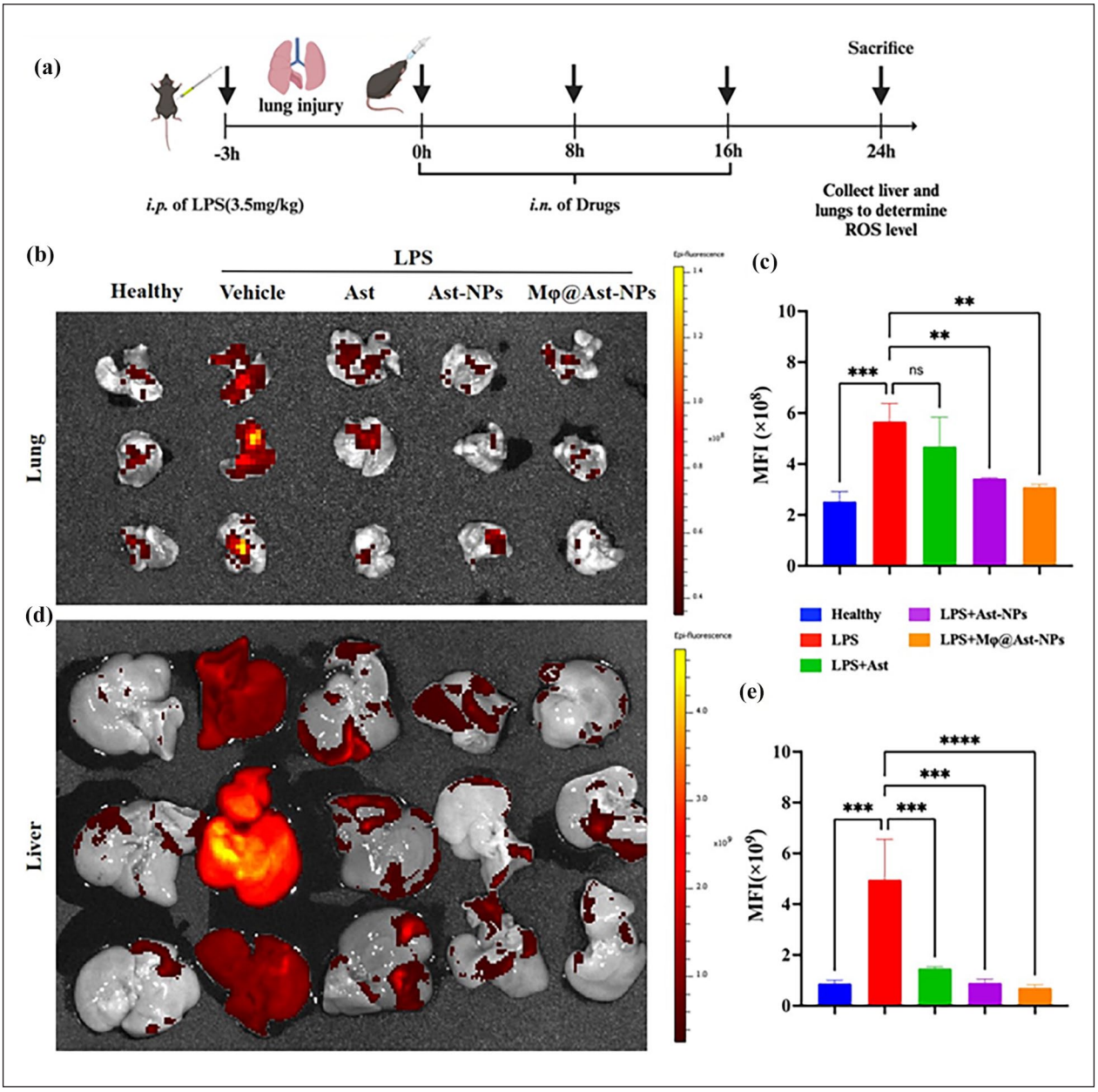

Figure 8. In vivo ROS scavenging activity of different formulations of Ast determined by DCF-HA staining. (a) Time axis of LPS-induced ALI and the timing of treatment: Mice were adaptively fed for one week, then i.p. of LPS to induce ALI model, after 3 h, the mice were i.n. administrated with different formulations of Ast at 400 μg/kg for three times (8 h for single dose). At 24 h post LPS challenge, the mice were sacrificed and collected livers and lungs for ROS determination. (b) The fluorescent pictures of lungs originated from differently treated ALI mice stained with DCF-HA kits imaged by an IVIS imaging system. (c) Relative MFI of DCF-HA in lung tissues of measured with Living Image 4.5 software. (d) The fluorescent pictures of livers originated from differently treated ALI mice stained with DCF-HA kits imaged by an IVIS imaging system. (e) Relative MFI of DCF-HA in livers. *$p < 0.05$, **$p < 0.01$, ***$p < 0.001$, ****$p < 0.0001$, ns, no significant differences ($n = 5$).

ALI pneumonia (Figures 8a). In vivo findings indicated that intranasal administration of free Ast exhibited limited ROS-scavenging ability compared to that of Ast-NPs and Mϕ@Ast-NPs (Figures 8(b) and (d)). Additionally, the quantitative statistical data in Figure 8(c) and (e) demonstrated that all formulations of Ast, including free Ast, exhibited remarkable ROS-scavenging properties. This suggests that the antioxidant activity and therapeutic effectiveness of Ast were notably enhanced by loading it into the biomimetic nano-platform, particularly in the lungs. Moreover, Ast-NPs, particularly Mϕ@Ast-NPs, exhibited significant ROS-scavenging capabilities.

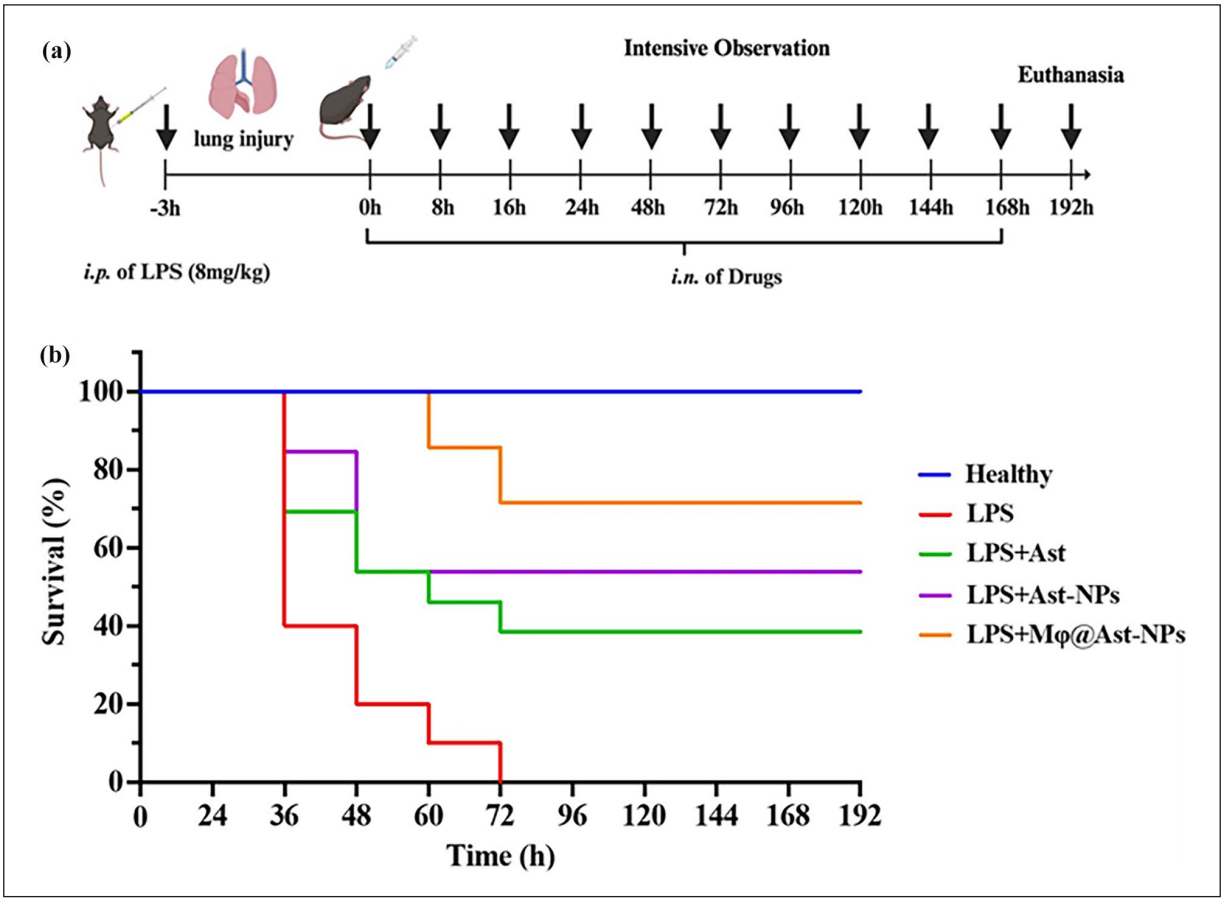

Figure 9. Survival rates of mice. Mice were pretreated with different formulations of Ast (400 μg/kg) 3 h before intraperitoneal injection with LPS at lethal dose (8 mg/kg body weight), 8 h for one dose. All the mice were under intensive observation for 7 days to record the survival rate ($n = 10$/group).

Survival rates of mice

To evaluate the survival benefits of different formulations of Ast, we employed a standard ALI mouse model induced by a lethal dose of lipopolysaccharide (LPS) at 8.0 mg/kg body weight. Prior to the LPS challenge, 3 h before administering the lethal dose, mice received a single intranasal (*i.n.*) dose of 400 μg/kg of Ast, Ast-NPs, or Mϕ@Ast-NPs every 8 h (as illustrated in Figure 9(a)) and were closely monitored thereafter. All mice in the ALI group treated with phosphate-buffered saline (PBS) succumbed within 48 h, confirming the successful establishment of the ALI model. Among those treated with free Ast, only 40% of the mice survived, while the survival rate was 50% in the Ast-NPs group. In contrast, administration of Mϕ@Ast-NPs significantly improved the protective effect, boosting the survival rate to 70% (as depicted in Figure 9(b)). These findings suggest that Mϕ@Ast-NPs can substantially enhance therapeutic efficacy and survival outcomes in ALI mice. Moreover, this biomimetic nanoparticle platform presents a promising intranasal drug delivery system for the treatment of ALI.

In vivo biosafety of different formulations of Ast

To evaluate the in vivo biosafety of different Ast formulations, we performed histological examinations on the major organs extracted from ALI mice treated with various formulations. The organs were stained with hematoxylin and eosin (H&E) to assess any potential histopathological changes. The histological analysis, as depicted in Figure 10(a), revealed no significant differences in the morphology of the main organs among all treatment groups. Furthermore, liver function assays, including measurements of ALT and aspartate aminotransferase (AST) and alanine aminotransferase (ALT), showed no notable changes (as depicted in Figure 10(b) and (c)). Further, the no-drug loaded macrophage membrane coated PLGA blank nanoparticles (Mφ@NPs) using healthy mice, the mice were intranasal administrated with Mφ@NPs for three times (8 h/once), there was no significant toxic effects in liver functions and histological sections. Taken together, these findings emphasize the biosafety of both Ast-NPs and Mϕ@Ast-NPs in the context of treating ALI.

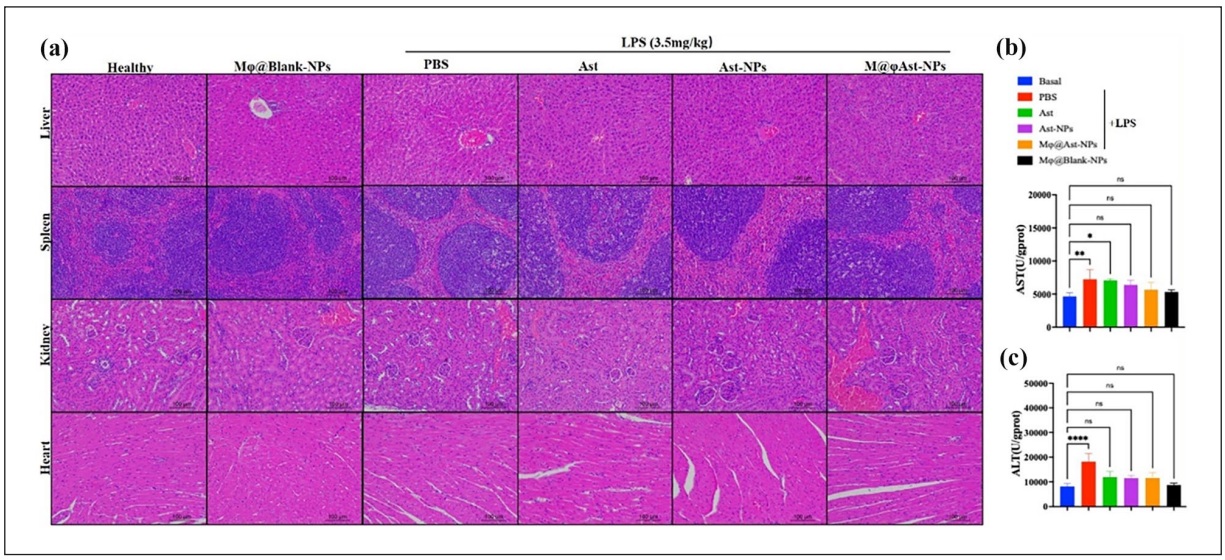

Figure 10. In vivo biosafety of different formulations of Ast. (a) Typical photos of main organs originated from ALI mice treated with different formulations of Ast. About 1 bar: 100 μm. (b and c) The levels of alanine transaminase (ALT) and aspartate transaminase (AST) of livers in each group were tested to evaluate the toxicity of different formulations of Ast, respectively. $^{*}p < 0.05$, $^{**}p < 0.01$, $^{***}p < 0.001$, $^{****}p < 0.0001$, ns, no significant differences ($n = 5$).

Conclusions

In conclusion, we developed a macrophage membrane-coated nanoplatform for delivering antioxidant drugs or compounds for pneumonia treatment. The synthesized Mϕ@Ast-NPs demonstrated exceptional biocompatibility, inflammation targeting, and enhanced anti-inflammatory efficacy both in vitro and in vivo. These NPs could evade immune system clearance and effectively accumulate in inflamed lungs in septic mice. In an LPS-induced ALI mouse model, Mϕ@Ast-NPs significantly increased survival rates, reduced cytokine levels in BALF and lungs, and attenuated ROS production. Mechanistic analysis indicated that the improved therapeutic effects of Mϕ@Ast-NPs may be attributed to the activation of Nrf2/HO-1 in macrophages. Importantly, the effective dose of Ast used in our study (400 μg/kg administered intranasally three times) was over 50 times lower than doses reported in previous studies (20 mg/kg administered intravenously for 7 days). Our findings underscore the potential of targeted drug delivery for ALI treatment in reducing cytokine storm syndromes compared to free drug therapy. This strategy holds promise as a nanoplatform for targeted pulmonary treatment and has potential applications in functional foods.

Macrophage cell membrane cloaked biomimetic astaxanthin PLGA (poly(lactic-co-glycolic acid)) nanoparticles represent an innovative approach for treating acute lung injury (ALI) and other respiratory conditions.[19] Key considerations for clinical application include: Firstly, enhanced Targeting: Macrophage membrane cloaked nanoparticles can significantly improve targeting specificity toward inflammatory sites in the lungs, which may enhance therapeutic efficacy while minimizing side effects of the encapsulated drugs. Various therapeutic agents, including small molecules, proteins, or RNA-based therapeutics, can be incorporated into these nanoparticles, potentially broadening their applicability to a range of respiratory diseases. Secondly, reduction of Immune Rejection: Utilizing the patient's own macrophage membranes to modify astaxanthin nanoparticles may significantly reduce the risk of immune rejection, facilitating safer clinical applications. Thirdly, application in Chronic Respiratory Diseases: Beyond ALI, exploring the use of these biomimetic nanoparticles for chronic respiratory diseases such as asthma, chronic obstructive pulmonary disease (COPD), and pulmonary fibrosis could yield substantial benefits. Fourthly, real-time Imaging and Tracking: Incorporating imaging modalities to monitor the distribution and behavior of these nanoparticles in vivo can provide valuable insights into their mechanisms of action and inform improvements in their design. By pursuing these directions, researchers can harness the potential of biomimetic nanoparticles to develop novel therapies for various respiratory conditions, ultimately improving patient outcomes.

Declaration of conflicting interests

The author(s) declared no potential conflicts of interest with respect to the research, authorship, and/or publication of this article.

Funding

The author(s) disclosed receipt of the following financial support for the research, authorship, and/or publication of this article:

This work was supported by the Natural Science Foundation of Guangdong Province (2022A1515140154), the Science Foundation of Dongguan Science and Technology Bureau (20231800940172), the Scientific research project of general universities in Guangdong province (2021KTSCX033), Guangdong Medical University post doctor Fund (1026/4SG23180G), and Guangdong Provincial Medical Research Fund (A2024676). Construction Project of Nano Technology and Application Engineering Research Center of Guangdong Medical University (4SG24179G). Figure 1 was created in https://BioRender.com, and agreement No. is BP27L12JO5.

ORCID iD

Hua Jin https://orcid.org/0000-0001-5478-4611

References

1. Jin GZ, Chakraborty A, Lee JH, et al. Targeting with nanoparticles for the therapeutic treatment of brain diseases. *J Tissue Eng* 2020; 11: 1–13.
2. Meyer NJ, Gattinoni L and Calfee CS. Acute respiratory distress syndrome. *Lancet* 2021; 398: 622–637.
3. Zhu W, Zhang Y and Wang Y. Immunotherapy strategies and prospects for acute lung injury: Focus on immune cells and cytokines. *Front Pharmacol* 2022; 13: 1103309.
4. Chang X, Li S, Fu Y, et al. Safety and efficacy of corticosteroids in ARDS patients: a systematic review and meta-analysis of RCT data. *Respir Res* 2022; 23: 301.
5. Georgieva E, Ananiev J, Yovchev Y, et al. COVID-19 complications: oxidative stress, inflammation, and mitochondrial and endothelial dysfunction. *Int J Mol Sci* 2023; 24: 14876.
6. Diao Y, Ding Q, Xu G, et al. Qingfei litan decoction against acute lung injury/acute respiratory distress syndrome: the potential roles of anti-inflammatory and anti-oxidative effects. *Front Pharmacol* 2022; 13: 857502.
7. Ambati RR, Phang SM, Ravi S, et al. Astaxanthin: sources, extraction, stability, biological activities and its commercial applications—a review. *Mar Drugs* 2014; 12: 128–152.
8. Luo L, Huang F, Zhong S, et al. Astaxanthin attenuates ferroptosis via Keap1-Nrf2/HO-1 signaling pathways in LPS-induced acute lung injury. *Life Sci* 2022; 311: 121091.
9. Dong X, Li D, Fang Z, et al. Astaxanthin alleviates lipopolysaccharide-induced acute lung injury by suppressing ferroptosis. *Food Funct* 2023; 14: 6115–6127.
10. Bi J, Cui R, Li Z, et al. Astaxanthin alleviated acute lung injury by inhibiting oxidative/nitrative stress and the inflammatory response in mice. *Biomed Pharmacother* 2017; 95: 974–982.
11. Nagendraprabhu P and Sudhandiran G. Astaxanthin inhibits tumor invasion by decreasing extracellular matrix production and induces apoptosis in experimental rat colon carcinogenesis by modulating the expressions of ERK-2, NFkB and COX-2. *Invest New Drugs* 2011; 29: 207–224.
12. Chen S, Wang J, Feng J, et al. Research progress of Astaxanthin nano-based drug delivery system: Applications, prospects and challenges? *Front Pharmacol* 2023; 14: 1102888.
13. Dash P, Piras AM and Dash M. Cell membrane coated nanocarriers – an efficient biomimetic platform for targeted therapy. *J Control Release* 2020; 327: 546–570.
14. Yoo SH, Kim HW and Lee JH. Restoration of olfactory dysfunctions by nanomaterials and stem cells-based therapies: current status and future perspectives. *J Tissue Eng* 2022; 13: 1–14.
15. Fang RH, Gao W and Zhang L. Targeting drugs to tumours using cell membrane-coated nanoparticles. *Nat Rev Clin Oncol* 2023; 20: 33–48.
16. Khatoon N, Zhang Z, Zhou C, et al. Macrophage membrane coated nanoparticles: a biomimetic approach for enhanced and targeted delivery. *Biomater Sci* 2022; 10: 1193–1208.
17. Shen S, Han F, Yuan A, et al. Engineered nanoparticles disguised as macrophages for trapping lipopolysaccharide and preventing endotoxemia. *Biomaterials* 2019; 189: 60–68.
18. Thamphiwatana S, Angsantikul P, Escajadillo T, et al. Macrophage-like nanoparticles concurrently absorbing endotoxins and proinflammatory cytokines for sepsis management. *Proc Natl Acad Sci USA* 2017; 114: 11488–11493.
19. Wu Y, Wan S, Yang S, et al. Macrophage cell membrane-based nanoparticles: a new promising biomimetic platform for targeted delivery and treatment. *J Nanobiotechnol* 2022; 20: 542.
20. Jin H, Pi J, Zhao Y, et al. EGFR-targeting PLGA-PEG nanoparticles as a curcumin delivery system for breast cancer therapy. *Nanoscale* 2017; 9: 16365–16374.
21. Xiao T, He M, Xu F, et al. Macrophage membrane-camouflaged responsive polymer nanogels enable magnetic resonance imaging-guided chemotherapy/chemodynamic therapy of orthotopic glioma. *ACS Nano* 2021; 15: 20377–20390.
22. Han M, Ma J, Ouyang S, et al. The kinase p38alpha functions in dendritic cells to regulate Th2-cell differentiation and allergic inflammation. *Cell Mol Immunol* 2022; 19: 805–819. 2022/05/14. DOI: 10.1038/s41423-022-00873-2.
23. Liu X, Li Y, Zhang W, et al. Inhibition of cIAP1/2 reduces RIPK1 phosphorylation in pulmonary endothelial cells and alleviate sepsis-induced lung injury and inflammatory response. *Immunol Res* 2024; 72(4): 841–850.
24. Shan H, Gao X, Zhang M, et al. Injectable ROS-scavenging hydrogel with MSCs promoted the regeneration of damaged skeletal muscle. *J Tissue Eng* 2021; 12: 1–15.
25. Zhang X, Shaukat M, Liu R, et al. Orally administered dual-targeted astaxanthin nanoparticles as novel dietary supplements for alleviating hepatocyte oxidative stress. *Food Funct* 2024; 15: 2131–2143.
26. Shang J, Liang T, Wei D, et al. Quercetin-loaded PLGA nanoparticles coating with macrophage membranes for targeted delivery in acute liver injury. *Nanotechnology* 2023; 35: 115102.
27. Stater EP, Sonay AY, Hart C, et al. The ancillary effects of nanoparticles and their implications for nanomedicine. *Nat Nanotechnol* 2021; 16: 1180–1194.
28. Gea-Sorli S, Guillamat R, Serrano-Mollar A, et al. Activation of lung macrophage subpopulations in experimental acute pancreatitis. *J Pathol* 2011; 223: 417–424.
29. Chen X, Tang J, Shuai W, et al. Macrophage polarization and its role in the pathogenesis of acute lung injury/acute

respiratory distress syndrome. *Inflamm Res* 2020; 69: 883-895. 20200710. DOI: 10.1007/s00011-020-01378-2.
30. Lim EY, Lee SY, Shin HS, et al. Reactive oxygen species and strategies for antioxidant intervention in acute respiratory distress syndrome. *Antioxidants* 2023; 12: 2016.
31. Shen K, Jia Y, Wang X, et al. Exosomes from adipose-derived stem cells alleviate the inflammation and oxidative stress via regulating Nrf2/HO-1 axis in macrophages. *Free Radic Biol Med* 2021; 165: 54–66.
32. Zhao Y, Jin H, Lei K, et al. Oridonin inhibits inflammation of epithelial cells via dual-targeting of CD31 Keap1 to ameliorate acute lung injury. *Front Immunol* 2023; 14: 1163397.
33. Davinelli S, Saso L, D'Angeli F, et al. Astaxanthin as a modulator of Nrf2, NF-kappaB, and their crosstalk: molecular mechanisms and possible clinical applications. *Molecules* 2022; 27: 502.
34. Cheng J and Eroglu A. The promising effects of astaxanthin on lung diseases. *Adv Nutr* 2021; 12: 850–864.
35. Xia T, Fu S, Yang R, et al. Advances in the study of macrophage polarization in inflammatory immune skin diseases. *J Inflamm* 2023; 20: 33.
36. Luo M, Yuan Q, Liu M, et al. Astaxanthin nanoparticles ameliorate dextran sulfate sodium-induced colitis by alleviating oxidative stress, regulating intestinal flora, and protecting the intestinal barrier. *Food Funct* 2023; 14: 9567–9579.